

Active optics and control architecture for a Giant Segmented Mirror Telescope

George Z. Angeli^{1*}, Myung K. Cho¹, Mark S. Whorton²

¹New Initiatives Office, AURA Inc., ²NASA Marshall Space Flight Center

ABSTRACT

The next generation 30-meter class ground-based telescopes pose an unprecedented challenge for control systems envisioned to support diffraction limited imaging. Our approach is a multi-tiered, decentralized control architecture utilizing two kinds of feedback: optical and mechanical. Based on simulations, we suggest a configuration where the optical feedback loops for the main axes, secondary mirror rigid body motions and segmented primary mirror are separated in both temporal and spatial frequency domains. The active optics system maintaining the continuity and higher order shape of the primary mirror is based on mechanical sensors while the low order shape is corrected through optical feedback. Shown are the results of numerical simulations using real, measured wind data that prove the feasibility of the suggested architecture.

Keywords: active optics, telescope control, segmented mirror control

1. INTRODUCTION

To meet the performance requirements, a successful 30-meter class telescope requires (i) active control of the telescope structure and optical surfaces, and (ii) adaptive correction to account both for wavefront distortions wrought by the atmosphere and for the effects of wind buffeting. The control architecture presented in this paper is valid for the most important operation domain, guide star tracking and image quality correction during observation. This procedure is the one that ultimately enables the utilization of the unique features of a 30-meter class telescope. Other operation domains, like high speed slewing and acquisition, require somewhat different control models. Furthermore, the specification requirements for these operation domains are much less stringent and the processes themselves are much less complex.

The active optics control of a large segmented mirror telescope represents substantial challenges:

- The primary mirror constitutes both a considerable bluff-body as well as an airfoil in the way of the wind. The stochastic pressure on the primary mirror reflects the turbulent characteristics of the incoming wind as well as local effects¹⁻³. The wind inflicts significant forces on the mirror surface, causing deformation, which, in turn, degrade the phasing of the mirror and potentially excite resonant modes of the telescope structure.
- The continuity of the primary mirror, as well as the overall shape of the mirror, should be maintained at least during the observation but preferably for a longer period, since the phasing procedure is complex and time consuming. The wind spectrum is partially overlapped with the structural resonances, which may result in cross talk between the continuity maintenance system and other structure control loops.
- The relatively large secondary mirror structure is also well exposed to the wind. Its stochastic motion due to wind forces directly influences the telescope aberrations, and also generates primary mirror tilts and deformations through the secondary support tripod. Both should be corrected, and again, partly inside the bandwidth of structural resonances.
- There is significant cross coupling between the optical elements of the telescope through both the optical and mechanical systems. The structure carries energy from one element to the other by means of the modal resonances. Meanwhile, the aberrations of the optical system are multiple-valued functions of the structural deformations, meaning different telescope configurations can result in very similar aberrations. With wavefront measurements restricted to a limited spatial frequency band, - which is the usual case due to limited guide star magnitudes, - it may be a significant challenge to discriminate between these deformations.

* gangeli@gemini.edu; phone 520-318-8413; AURA New Initiatives Office, 950 N. Cherry Ave., Tucson, AZ, USA 85719.

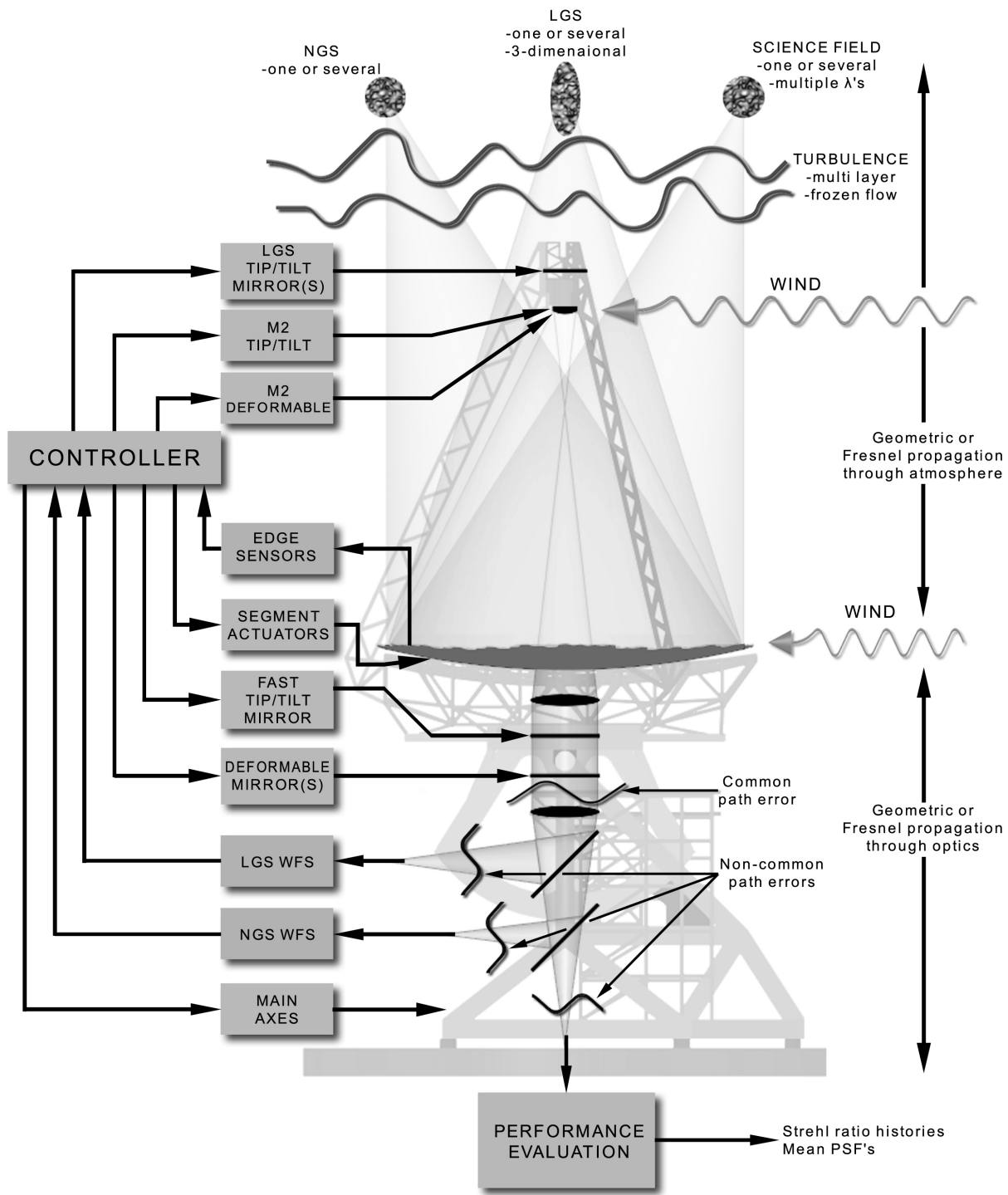


Figure 1. Sensors and actuators of a Giant Segmented Mirror Telescope (including AO)

To correct the aberrations, the current status of the telescope should be sensed and then the system should be commanded toward the desired status by means of actuators. Without going into the details of this here, we list the information and stimuli necessary to control the telescope (*Figure 1*).

Actuator groups:

- Main axes, as the elevation and azimuth of the telescope;
- Segmented primary mirror active control to tip, tilt, and piston the individual segments, as well as rafts;
- Secondary mirror rigid body motion, as of tip, tilt, x, y and z translation;
- Deformable secondary mirror face-sheet;
- Other high resolution deformable mirrors after the secondary mirror for high order adaptive optics (AO) systems, like MCAO or adaptive coronagraph.

Sensor groups:

- Optical detectors like wavefront sensors to measure the wavefront aberrations;
- Mechanical detectors, like segment edge sensors or inertial sensors to measure the status of the mechanical structure.

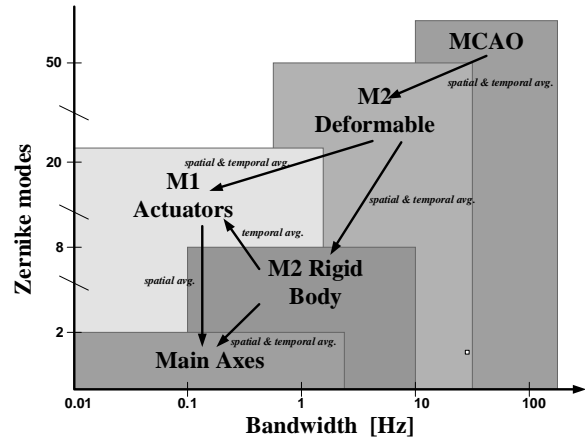


Figure 2: Temporal and spatial frequency bands of different actuator groups

The capabilities of different actuator groups to influence the image quality are well bounded both in temporal and spatial frequency, as shown in *Figure 2*. The redundancy in image correction is apparent from the overlapping areas of various actuator groups.

2. CONTROL ARCHITECTURE

In order to define a feasible control architecture, first we should investigate the amplitude and frequency range of different disturbances acting on the telescope. There are four major sources of disturbances: (i) the gravitational deformation of the telescope, (ii) the thermal expansion of the telescope, (iii) the wind induced deformation of the telescope, and (iv) the wavefront deformation due to atmospheric turbulence. Fully understanding the effects of these sources on the image quality of a 30-meter class telescope needs significant amount of further investigation and simulations. However, at this point our major concern is the general architecture of the control system and not the detailed design of the individual feedback loops.

The control architecture about to be described here is based on a pivotal assumption; namely there is no high frequency disturbance with reasonable power that tends to break the continuity of the segments on the primary mirror. In other words, the segment actuators can be operated slow enough – below the resonant frequencies of the structure - to avoid interactions with the structural dynamics. Let us see now whether the characteristics of various disturbances support this assumption.

The thermal effects are potentially large but tend to be rather slow. The temperature changes on a mountaintop during the night are usually very slow. Considering a 1°C/hour maximum temperature gradient and 5°C swing, the bandwidth of this disturbance is less than $2 \cdot 10^{-5}$ Hz.

The major gravitational effect on the primary mirror is axial deformation, since the lateral motion of the segments is not going to destroy the continuity of the mirror – as long as the segments are not crushing into each other, of course. These gravity effects due to sidereal tracking repeat at diurnal frequency, so the bandwidth can be estimated as about 10^{-5} Hz.

Assuming smooth enough bearings, actuators and sensors, during sidereal tracking the correction of thermal and gravitational deformations should not interact with the structural dynamics of the telescope. However, later in the design process different service bandwidths should be defined that characterize and bound the speed of other telescope operations, like settling after slewing, pointing, offsetting, scanning.

The refraction index fluctuations in the atmosphere obviously don't influence the shape of the telescope, but their effects appear in the optical measurements meant to determine that shape. Some of the atmospheric effects will be corrected by the telescope active optics system due to their inseparability from telescope deformations. Since the telescope deformations are expected to be measured with a single – most likely natural - guide star, the refractive wavefront deformations will be corrected only in the isoplanatic patch around that guide star. In case of using MCAO wavefront sensors though, the ground layer turbulence is the one that is not separable from the telescope deformations.

There are significant telescope deformations induced by the wind. The wind forces acting on the structure and optical surfaces feature high enough bandwidth to interact with the structural dynamics of the telescope. The magnitude and bandwidth, as well as the observability and controllability of the wind-induced deformations are investigated by means of computer simulations in a later section of this paper.

The general control model shown in *Figure 3* integrates the mechanical, optical and control subsystems of the telescope, as well as the external disturbances. It is worth mentioning, that while the wind and the gravitational and thermal effects affect the image quality through structural deformations, the virtual sky motion and the atmospheric turbulence show up in the light itself. The control system features two distinct feedback loops, based on the two groups of sensors.

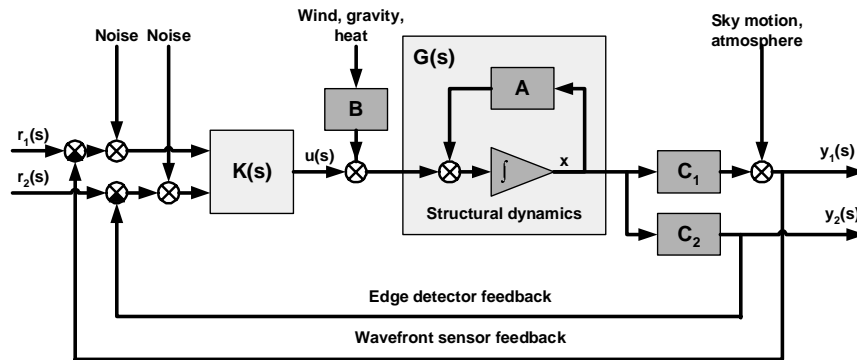


Figure 3: Control configuration (including AO)

The command signal $r_1(s)$ for the optical feedback loop is the constant aberration of the un-deformed telescope, mainly due to the off-axis position of the guide star. The command signal $r_2(s)$ for the edge detector feedback loop corresponds to the perfect positions of the primary mirror segments determined by phasing the mirror.

This model does not contain pertinent information on “boot strapping” the control system, that is, locking it on the guide star. The locking procedure involves not only nonlinear but also time dependent transient processes and it needs to be investigated further in the future.

Although a fully centralized global controller (as shown in *Figure 3.*) offers advantages that are worthy of pursuit, such as the capability to account for the full complexity of the telescope system and interaction between sensor/actuator groups, there are practical limitations with a global controller of this nature. In view of implementation issues, such as uncertainties in the dynamics of the structure, large dimensional state dynamics, and computational complexity, a decentralized approach that decouples the major control loops is pursued in this paper. Within the context of the decoupled and decentralized subsystem control loops, modern control methods are applicable and potentially well suited⁴. Forced decoupling of the otherwise interacting subsystems presents an opportunity for a decentralized control architecture that provides several benefits over a centralized one:

- It simplifies the cost functions and the consequent control laws to be designed and implemented;
- It improves the understanding of underlying concepts and processes;
- It supports detached, step-by-step design, implementation and troubleshooting of the subsystems.

Based on the assumption of separability of segment alignment and structural dynamics, a distributed telescope control architecture can be outlined. The continuity of the segmented primary mirror is maintained by a system utilizing edge

detector information about the shape of the mirror. Since the lowest order modes of the structure have resonant frequencies around 2 Hz^5 , the bandwidth of the continuity maintenance system should be significantly less than 2 Hz in order to avoid actuator-structure interactions.

A continuous primary mirror does not guarantee an aberration-free telescope, though. The shape of the primary mirror still can be deformed just as other parts of the telescope structure. Our choices are either further observing the structural deformations and correcting them when and where they occur, or extracting information from the aberrated wavefront and arranging a hierarchical correction scheme mostly independent of the actual location of the deformation. The latter method has the inevitable advantage of directly observing and controlling the single most important characteristics of the telescope: its optical quality.

The optical feedback system has three actuator groups: (i) the secondary rigid body motion, (ii) the primary mirror segments, and (iii) the main axes. The somewhat arbitrarily defined separation of these subsystems in spatial and temporal frequencies is shown in *Figure 4*. The bandwidths for primary shape and the main axes controls were established so that their separation from the structural dynamics is ensured as much as possible.

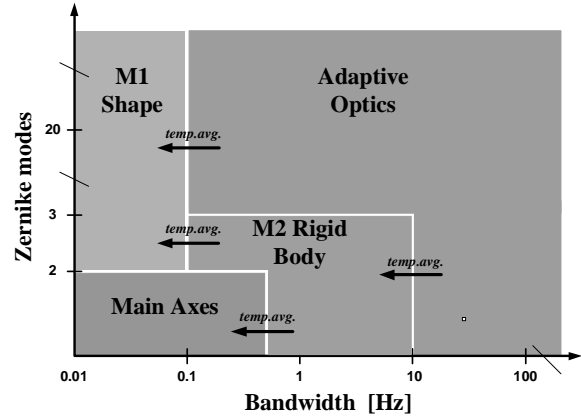


Figure 4: Frequency band separation of wavefront correction

From the point of view of control architecture, a conventional AO system – like the direct Cassegrain AO or AO coronagraph for GSMT - will have two major actuator groups: the deformable secondary mirror and the higher-order deformable mirrors. The deformable secondary mirror is inherently part of the telescope control system as well, because any wavefront sensor detecting the telescope deformation is also detecting the wavefront correction imposed by the secondary. On the other hand, the higher-order mirrors can be de-coupled from the telescope control by a sensible arrangement of WFSs, where the first high-order AO sensor is downstream of the last telescope control actuator in the light path. As long as the residual OPD is small enough in amplitude after all the telescope shape corrections, the high-order AO system - with its superior resolution and bandwidth - can presumably handle any misalignment possibly generated by the rest of the control system. Consequently, the high-order AO systems can be considered independent of the telescope control and are beyond the scope of this paper.

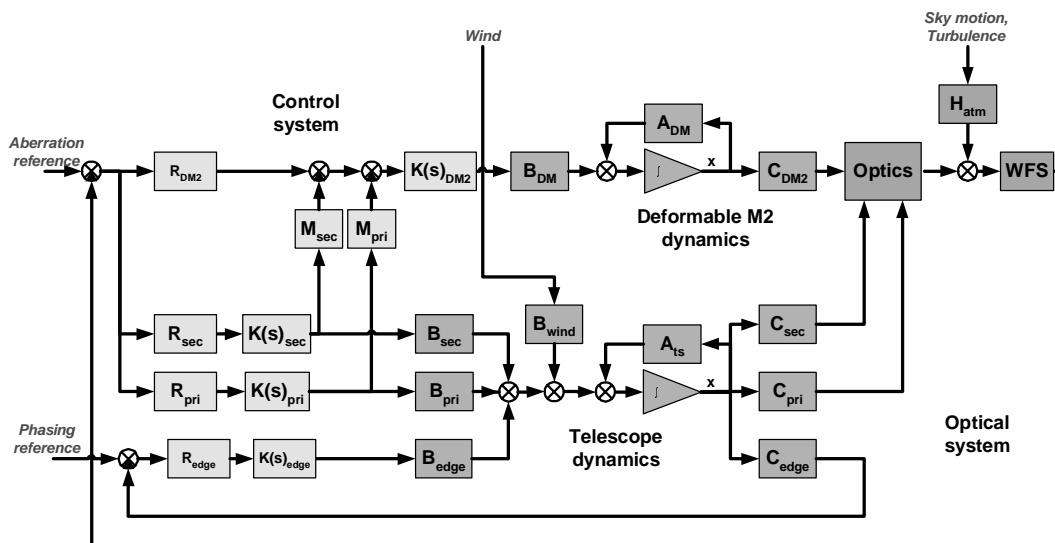


Figure 5. Decentralized control configuration (including adaptive secondary but omitting the main axes)

In the MCAO reconstructing scheme, the ground layer turbulence is inseparable from the telescope deformations. This will inevitably lead to a tighter integration of AO and telescope control, where the control commands for the adaptive secondary are off-loaded from the whole reconstructed ground layer through modal and temporal filters.

The decentralized control configuration is shown in *Figure 5*. The centralized controller is distributed into four separate reconstructors and controllers. Each reconstructor \mathbf{R} incorporates also a modal (spatial) filter to ensure that the individual actuator groups are not fed with inappropriate spatial information. The temporal filters, required for decoupling, are realized as part of the controllers $\mathbf{K}(s)$.

Instead of relying entirely on the modal and temporal filters to accomplish the perfect mesh of controls, a subtraction scheme is suggested. In this scheme the adaptive optics reconstructor \mathbf{R}_{DM2} estimates the required control actions in their fullest possible extent and the corrections made by limited spatial and temporal bandwidth controllers are subtracted from it. Obviously, the subtraction can be done only after converting these corrections into the modal space of the deformable secondary mirror (by multiplying with \mathbf{M}_{pri} and \mathbf{M}_{sec}). For the sake of clarity, the main axes are omitted in *Figure 5*. Their treatment is analogous to those of the primary and secondary mirror optical control loops.

By enforcing the limited bandwidth of the primary mirror shape and continuity controls in the appropriate controllers, these loops become uncoupled from the structural dynamics of the telescope. The lack of dynamics in these loops drastically simplifies the control laws.

The thin glass facesheet of the deformable secondary mirror has negligible mass compared to the whole secondary assembly containing the reference body, support structures, and electronics. Thus, even the fast motions of the facesheet are not transferred to the telescope structure. Furthermore, a local control system is expected, which transforms the deformable secondary to position actuator. Consequently, from the telescope control point of view, the dynamics of the deformable secondary mirror can be neglected. That leaves only one loop, the secondary mirror rigid body motion control, with substantial control-structure interaction⁴.

3. SIMULATIONS

The adverse effect of wind on a giant telescope is aggravated by the fact that the larger the telescope the lower its resonant frequencies are, so it can absorb a significantly higher percentage of wind energy than a smaller one would. In order to investigate the effect of wind forces on the telescope structure, we have simulated the telescope structural dynamics using Matlab. As input we apply real, measured wind velocities and pressures recorded at the Gemini South Telescope in Chile¹.

To reduce the computational requirements, we took a two-step approach. The first round of simulations determined the dynamic deformations of the whole telescope structure and assessed the high order displacements of the primary mirror support. In the second step the individual segment rigid body motions were considered and evaluated, but without the impact of the whole structure. We intend to merge the two approaches in the future and report the results in subsequent papers.

3.1. Primary mirror structural deformation

We can assume, with good confidence, that the deformations of the structure are repeatable and linear functions of the forces acting on it. The customary representation of linear structures is based on structural modes, or eigenvectors⁶. The actual displacements are the linear combinations of these modes. Applying a special linear transformation of Φ – which is the system eigenvector matrix – on the Newtonian equations of motion of the structure, the differential equations become uncoupled.

$$\ddot{\mathbf{q}}_m + 2\mathbf{Z}\Omega\dot{\mathbf{q}}_m + \Omega\mathbf{q}_m = \mathbf{M}^{-1}\Phi^T\mathbf{B}_0\mathbf{u}$$

The external forces applied on the structure are represented by \mathbf{u} . The independence of the modal equations – i.e. the diagonality of the coefficient matrices \mathbf{M} , \mathbf{Z} and Ω – is the major advantage of modal representation. A further step toward a higher level of abstraction reduces the differential equations to first order.

$$\mathbf{x} = \begin{bmatrix} \mathbf{q}_m \\ \dot{\mathbf{q}}_m \end{bmatrix}$$

$$\dot{\mathbf{x}} = \begin{bmatrix} \mathbf{0} & \mathbf{I} \\ -\mathbf{\Omega}^2 & -2\mathbf{Z}\mathbf{\Omega} \end{bmatrix} \mathbf{x} + \begin{bmatrix} \mathbf{0} \\ \mathbf{M}^{-1}\mathbf{\Phi}^T\mathbf{B}_0 \end{bmatrix} \mathbf{u}$$

This so-called state-space representation of linear time-invariant systems is not just very visual, but also consistent with all the advanced tools of modern control theory⁷. Although these modern control methods are highly model dependent, there are well-developed techniques for addressing parameter uncertainties such as ambiguity in modal damping and frequency.

For simulation and design purposes, the finite element analysis (FEA) of the structure⁴ provides the coefficients $\mathbf{\Omega}$, \mathbf{Z} and \mathbf{M} , as well as the eigenvector matrix $\mathbf{\Phi}$.

In the telescope configuration associated with the particular wind measurement used for this simulation, the observing slit, as well as the ventilation gates on both sides were open. The telescope zenith angle was 30° and it was facing into the wind (case c00030o⁸).

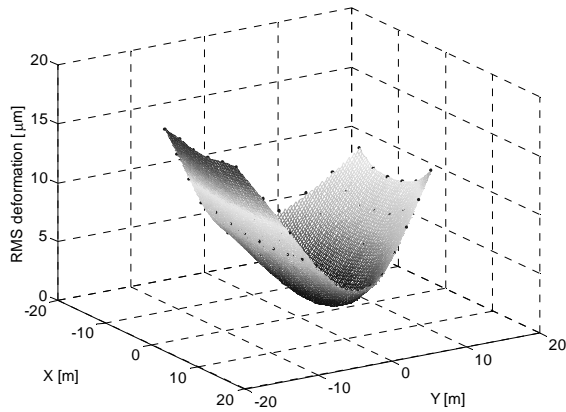


Figure 6: Primary mirror deformation due to wind load

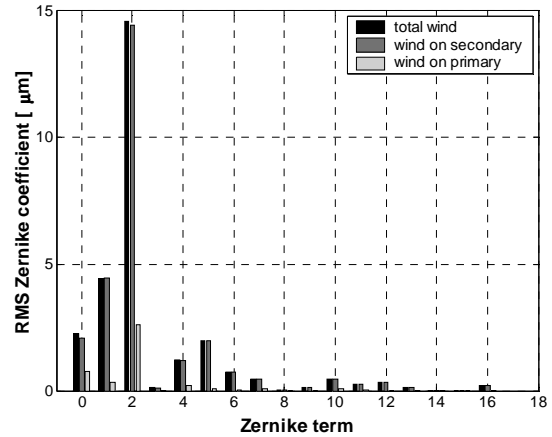


Figure 7: Zernike expansion of the primary mirror deformation

The mean wind velocity at the primary and secondary mirror was about 4 m/s, while outside of the dome it was about 11 m/s. Our analysis indicates that the data collected by the different pressure sensors on the Gemini dummy primary mirror are practically independent². Consequently, these pressure time series could be patched together (repeated for different node groups) to yield the simulation pressures on the 30-meter GSMT primary mirror. The resulting deformation – which was calculated as the temporal RMS of instantaneous displacements of each node - is shown in *Figure 6*.

The shape of the primary indicates that the deformation of the secondary structure has a major contribution while pressure variations on the primary mirror are less influential. The other important conclusion is that the overall structural deformation is dominated by low order modes. These facts are even more obvious from the Zernike expansion of the deformation, as it is shown in *Figure 7*.

The power spectrum density (PSD) of the RMS primary mirror deformation clearly shows the structural resonances around 2 Hz and 4 Hz (*Figure 8*). To evaluate the high order content of the deformations, the 1st, 3rd, 5th, 7th, 9th, and 11th order aberrations (up to Zernike term #36)⁹ were removed. Assuming close to perfect corrections up to a given frequency, the residual figure error can be calculated as the integral of the PSD curve from that given frequency to infinity. This residual error is shown in *Figure 9*, as the function of the correction bandwidth. At/above the frequency of 0.5 Hz the residual RMS figure error is about 32 nm. Even if we assume that all of this error is discontinuity, the value is favorably comparable to the requirements of the top-down error budget for GSMT⁴; it is also close to the actual measured closed loop discontinuities at the Keck Telescope¹⁰.

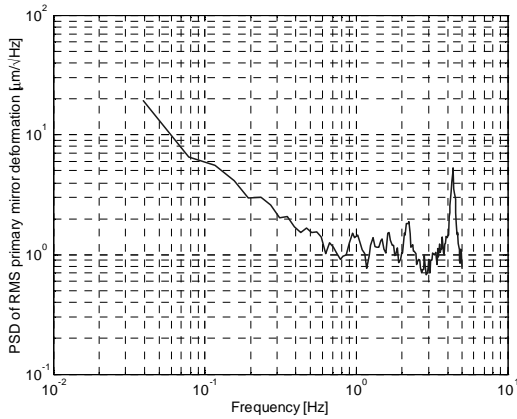


Figure 8. PSD of primary mirror deformation due to wind load (spatial RMS)

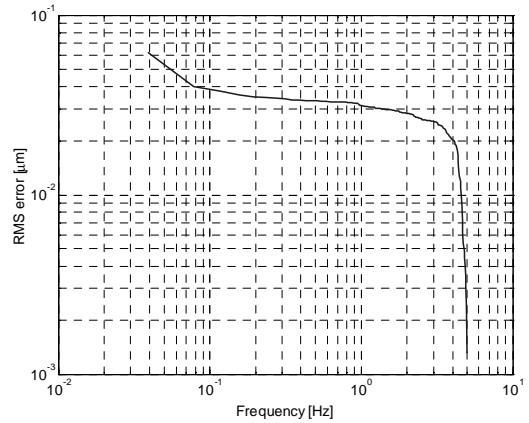


Figure 9. Residual RMS deformation at/above correction frequencies (first 37 Zernike terms removed)

3.2. Primary mirror segment alignment

According to our measurements at the Gemini South Telescope, the correlation length of the wind pressure variations on the primary mirror is less than 2 meter². Consequently, if we neglect the large-scale structural deformations, the wind-induced misalignments of the segments are effectively independent on different primary mirror areas with diameters of 5-8 meters. This allows us to use a Gemini size segmented mirror, instead of the whole GSMT mirror, for estimating the wind-induced misalignments. The advantage of this approach is twofold: (i) we don't have to manipulate the actual, measured wind data, and (ii) the calculations are less computation intensive.

The segment size for the “imaginary” Gemini segmented mirror was chosen the same as for the GSMT: 1.152 meter side to side³. Each segment is supported by three actuators. The structural model used contains only the stiffness of the segment actuators (10 N/μm), but no dynamics. The resonance frequencies of the segment-actuator systems (~60 Hz) are well above the range of interest in this simulation.

A static influence function \mathbf{G} can be defined for the primary mirror as the assembly of edge detector responses, $\mathbf{y}(\mathbf{s})$, to actuator pokes, $\mathbf{u}(\mathbf{s})$ (see Figure 10.). The singular value decomposition of the influence function yields actuator and sensor modes as basis vectors to any actuator command set and sensor reading group¹⁰. Each actuator mode, consisting of distinct positions for each actuator, has a corresponding sensor mode, (i.e., a unique set of sensor readings). There is a single scalar gain – the corresponding singular value of the influence function - for each actuator-sensor mode pair that characterizes the strength of the mirror response.

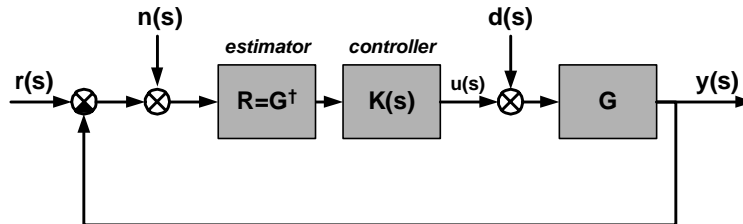


Figure 10. Primary mirror continuity control configuration

The feedback system that maintains the continuity and shape of the primary mirror performs two functions. First, as a reconstructor, it estimates hypothetical actuator forces that would result in the actual sensor readings. Then, as a controller, it feeds back the inverse of these forces to eliminate the deformation. The control configuration in Figure 10 also shows the wind forces $\mathbf{d}(\mathbf{s})$ acting on the segment surfaces and the sensor noise $\mathbf{n}(\mathbf{s})$. We introduced sensor noise with an RMS value of 10 nm and a bandwidth of 5 Hz, similar to the actual measured sensor noise at the Keck Telescope¹⁰, and also to the expected noise at CELT¹¹. In absence of strong noise and disturbances, the optimal reconstructor \mathbf{R} is the pseudo-inverse of the

influence function. The command signal $\mathbf{r}(\mathbf{s})$ is the optimal segment position determined by mirror phasing. In our simulation it's zero, since we can assume perfect edge sensor geometry without loss of generality.

Although the control is global in the sense that it collects all the edge sensor information and commands all the actuators according to a global control law, it can be conceived as a set of independent modal feedbacks. Because any actuator command set can be expressed as the linear combination of actuator modes, and the resulting sensor output can be assembled as the same linear combination of the corresponding sensor modes, we are concerned only with the mode propagation through the system. The assembly of the individual modal feedbacks is the control law realized by the reconstructor and controller. In our simulation case the controller $\mathbf{K}(\mathbf{s})$ is the same bandwidth limited proportional controller for all modes with a gain of 50 and bandwidth of 0.02 Hz.

In the actual configuration modeled, there are 108 actuators and only 84 edge sensors (one for each matching segment side pair). As a direct consequence, there are 24 unobservable actuator modes on the mirror. These unobservable modes, along with the barely observable ones (with small singular values), are going to show up in the shape of the mirror even when the control loop is closed (see *Figure 16.*). Even if we applied more edge sensors to avoid unobservable actuator modes, there would be several modes with very low singular values due to the inherent geometric restrictions of the edge sensors. These modes would still not be corrected properly by the mechanical feedback, which is why the optical feedback is unavoidable.

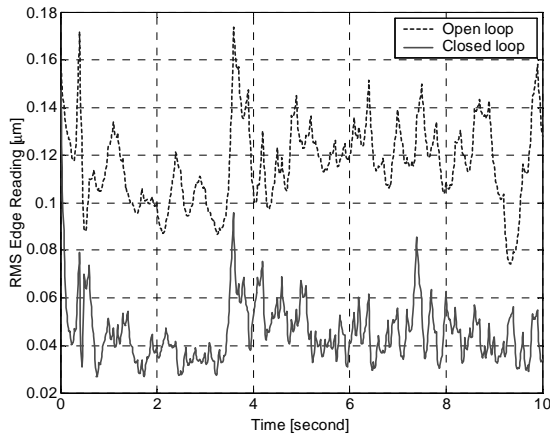


Figure 11. RMS edge sensor reading in open and closed loop (high wind)

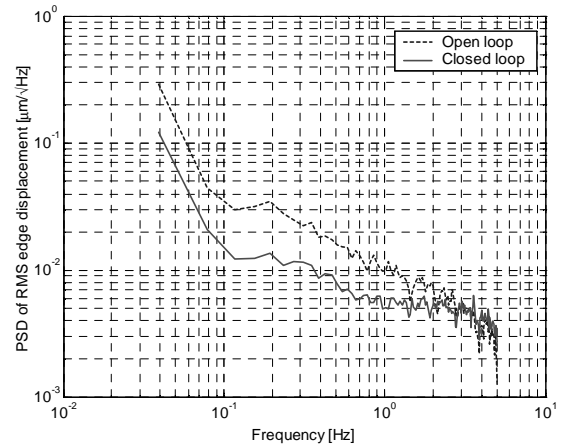


Figure 12. PSD of edge sensor reading in open and closed loop (high wind, $RMS_{open}=112nm$, $RMS_{closed}=45nm$)

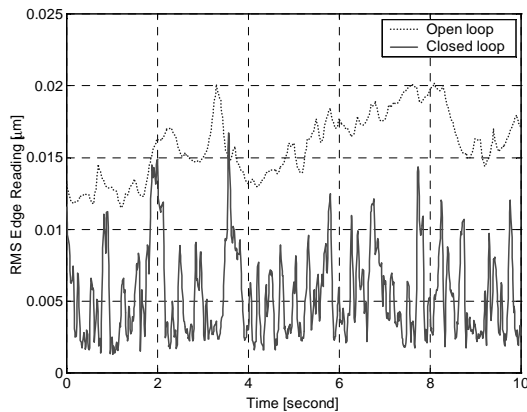


Figure 13. RMS edge sensor reading in open and closed loop (low wind)

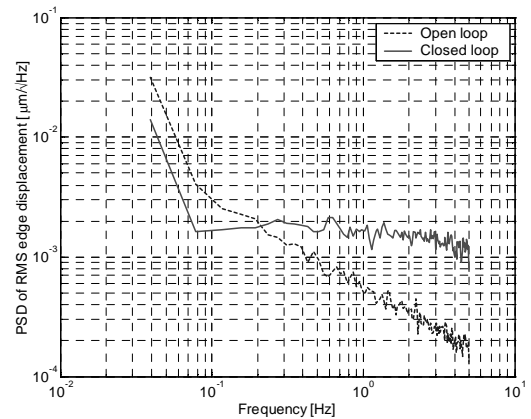


Figure 14. PSD of edge sensor reading in open and closed loop (low wind, $RMS_{open}=12nm$, $RMS_{closed}=6nm$)

The simulations were run for two cases, high and low wind. The high wind conditions were identical to the ones used for structural simulations: the ventilation gates and observing slit of the Gemini dome were open and the telescope was facing into the wind with a zenith angle of 30° . The time evolution of the spatial RMS of edge discontinuities is shown in *Figure 11* for open and closed control loops. The power spectral densities of these signals clearly show the effectiveness of the control (*Figure 12*).

The same telescope position with closed ventilation gates yields a characteristic low wind measurement set (c00030cc⁸). The average wind speed around the primary mirror was about 0.6 m/s. Using this low wind case as input, the time evolution signals in *Figure 13* are much smaller, as expected. The closed loop signal visibly shows the dominance of sensor noise. This dominance at higher frequencies (above 0.2 Hz) is even more obvious from the PSD curves (*Figure 14*). It is noteworthy that most of this noise is carried by lower order, barely observable modes. By filtering out these modes in the reconstructor, the noise level can substantially be reduced.

Characteristic snapshots of the primary mirror with open and closed control loops are shown in *Figures 15* and *16*. While in the open loop case the segment contours are clearly visible because of the discontinuities, in the closed loop case the deformations are much smoother, membrane-like. (The figures are not related.)

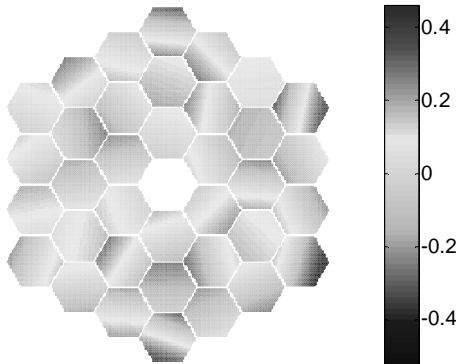


Figure 15: Primary mirror snapshot without phasing maintenance system (deformation in μm)

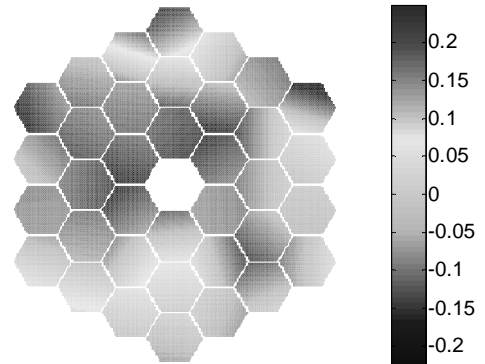


Figure 16: Primary mirror snapshot with phasing maintenance system (deformation in μm)

4. CONCLUSIONS

The simulation results reported in the preceding section clearly show the feasibility of a decentralized control architecture, which minimizes the control-structure interactions. A limited bandwidth primary mirror aO system is capable indeed of reducing the edge discontinuities to acceptable level even under high wind conditions. The shape control of the primary mirror is distributed between the active optics (for slow but long range shape corrections) and adaptive secondary systems (for high speed but short range corrections).

Under low wind conditions, the elimination of the edge discontinuities is trivial. However, the closed ventilation gates, resulting in low wind inside the dome, may also lead to insufficient flushing and cooling of the primary mirror and its close environment. This, in turn, increases “dome seeing” right in front of the mirror.

At the other extreme, our simulations highlight the general consensus among telescope builders that a large telescope without protective enclosure poses a major control challenge. The worst-case scenario reported in this paper features substantially higher wind speed around the primary mirror than those currently allowed at contemporary 10-meter class telescopes (2-3 m/s)³. However, these high wind velocities (~ 4 m/s) are already significantly attenuated compared to the wind speeds outside of the enclosure (~ 10 m/s).

Further investigations should balance the dome seeing with primary mirror deformation and discontinuity to determine the optimum wind conditions inside a telescope dome. These optimum conditions should minimize not only the amount of image aberrations inflicted, but also the bandwidth of these aberrations.

ACKNOWLEDGEMENTS

The authors would like to thank Brent L. Ellerbroek of the Gemini Observatory for his valuable suggestions and comments.

The New Initiatives Office is a partnership between two divisions of the Association of Universities for Research in Astronomy (AURA), Inc.: the National Optical Astronomy Observatory (NOAO) and the Gemini Observatory. NOAO is operated by AURA under cooperative agreement with the National Science Foundation (NSF). The Gemini Observatory is operated by AURA under a cooperative agreement with the NSF on behalf of the Gemini partnership: the National Science Foundation (United States), the Particle Physics and Astronomy Research Council (United Kingdom), the National Research Council (Canada), CONICYT (Chile), the Australian Research Council (Australia), CNPq (Brazil) and CONICET (Argentina).

REFERENCES

1. M. K. Cho, L. M. Stepp, S. Kim, "Wind Buffeting Effects on the Gemini 8m Primary Mirrors," *Proceedings of SPIE* **4444**, 302-314 (2001).
2. G. Z. Angeli, M. K. Cho, M. Sheehan, L. M. Stepp, "Characterization of Wind Loading of Telescopes," *Proceedings of SPIE* **4757**, 72-83 (2002).
3. M. K. Cho, L. M. Stepp, G. Z. Angeli, D. Smith, "Wind Loading of Large Telescopes," *Proceedings of SPIE* **4837**, (2002). to be published
4. M. Whorton, G. Z. Angeli, "Modern Control of the Secondary Mirror of a Giant Segmented Mirror Telescope," *Proceedings of SPIE* **4840**, (2002). to be published
5. *Enabling a Giant Segmented Mirror Telescope for the Astronomical Community*, (<http://www.aura-nio.noao.edu/book/index.html>, 2002).
6. W. K. Gawronski, *Dynamics and Control of Structures (A Modal Approach)*, (Springer-Verlag, New York, 1998).
7. S. M. Shinnars, *Advanced Modern Control System Theory and Design*, (John Wiley & Sons, New York, 1998).
8. *The Gemini South Wind Load Test*, (<http://www.aura-nio.noao.edu/studies/loading.html>, 2000)
9. J. C. Wyant, K. Creath, "Basic Wavefront Aberration Theory for Optical Metrology" in *Applied Optics and Optical Engineering XI*, (Academic Press, Boston, 1992)
10. M. Troy, G. Chanan, E. Sirko, E. Lefert, "Residual Misalignments of the Keck Telescope Primary Mirror Segments: Classification of Modes and Implications for Adaptive Optics," *Proceedings of SPIE* **3352**, 307-317 (1998).
11. T. S. Mast, J. E. Nelson, "Segmented Mirror Control System Hardware for CELT," *Proceedings of SPIE* **4003**, 226-240 (2000).